

RESEARCH ARTICLE

Improving MRI Resolution: A Cycle Consistent Generative Adversarial Network-Based Approach for 3T to 7T Translation

ZAKARIA SHAMS SIAM¹, RUBYAT TASNUVA HASAN²,
MOAJJEM HOSSAIN CHOWDHURY¹, MD. SHAHEENUR ISLAM SUMON³,
MAMUN BIN IBNE REAZ⁴, (Senior Member, IEEE),
SAWAL HAMID BIN MD ALI¹, (Senior Member, IEEE), ADAM MUSHTAK⁵,
ISRAA AL-HASHIMI⁵, SOHAIB BASSAM ZOGHOUL⁵, AND
MUHAMMAD E. H. CHOWDHURY³, (Senior Member, IEEE)

¹Department of Electrical, Electronic and Systems Engineering, Centre of Advanced Electronic and Communication Engineering, Universiti Kebangsaan Malaysia (UKM), Bangi, Selangor 43600, Malaysia

²Department of Mathematics and Physics, North South University, Dhaka 1229, Bangladesh

³Department of Electrical Engineering, Qatar University, Doha, Qatar

⁴Department of Electrical and Electronic Engineering, Independent University Bangladesh, Dhaka 1229, Bangladesh

⁵Department of Radiology, Hamad Medical Corporation, Doha, Qatar

Corresponding authors: Muhammad E. H. Chowdhury (mchowdhury@qu.edu.qa) and Mamun Bin Ibne Reaz (mamun.reaz@iub.edu.bd)

This work was supported in part by the Ministry of Higher Education (KPT), Malaysia, under Grant FRGS/1/2021/TK0/UKM/01/4; in part by Universiti Kebangsaan Malaysia (UKM) under Grant DIP-2020-004. Open Access funding is provided by the Qatar National Library.

ABSTRACT Brain magnetic resonance imaging (MRI) offers intricate soft tissue contrasts that are essential for diagnosing diseases and conducting neuroscience research. At 7 Tesla (7T) magnetic field intensity, MRI enables increased resolution, enhanced tissue contrast, and improved SNR, compared to MRI collected from the commonly employed 3 Tesla (3T) MRI scanners. However, the exorbitant expenses associated with 7T MRI scanners hinder their broad use in research and clinical facilities. Efforts are underway to develop algorithms that can generate 7T MRI from 3T MRI to achieve better image quality without the need for 7T MRI machines. In this study, we have adopted a cycle consistent generative adversarial network (CycleGAN)-based approach for 3T MRI to 7T MRI translation, and vice versa, using a recently published dataset of paired T1-weighted MR images collected at 3T and 7T from a total of ten subjects. Various CycleGAN architectures were experimented with and compared on this dataset. The best performing CycleGAN architecture successfully produced the reconstructed images with a high level of accuracy based on different quantitative and qualitative evaluation criteria. Utilizing a post-processing technique, the best performing model generated 7T MRI from 3T MRI with a structural similarity index measure (SSIM) of 83.80%, peak SNR (PSNR) of 26.25, normalized mean squared error (NMSE) of 0.0088 and normalized mean absolute error (NMAE) of 0.0630. Utilizing CycleGAN to convert images from 3T to 7T MRI has shown a substantial improvement in MRI resolution, setting the stage for advancements in more informative and precise diagnostic imaging.

INDEX TERMS Cycle consistent generative adversarial network, image-to-image translation, magnetic resonance imaging, paired dataset, T1-weighted MRI.

The associate editor coordinating the review of this manuscript and approving it for publication was Marco Giannelli¹.

I. INTRODUCTION

Medical imaging is essential for diagnosing and treating various illnesses. Multiple imaging modalities are typically used in clinical decision-making as they can offer complementary

insights. For instance, computed tomography (CT) provides essential physical density and electron density information of tissues for precise dosage planning in radiotherapy for cancer patients. However, CT has the drawback of poor contrast especially in soft tissues [1], [2]. Radiation exposure at the time of imaging can elevate the likelihood of subsequent malignancy, particularly in young individuals [1], [2]. On the contrary, as a non-invasive technique, magnetic resonance imaging (MRI) provides excellent contrast for soft tissues. Three-dimensional MRI of the human brain provide extensive information on its structure, essential for assessing brain morphology, investigating brain development, and identifying neurodevelopmental and neurodegenerative problems [3]. MRI is safer than CT because it does not entail radiation, however, it is more expensive and lacks the density information required for positron emission tomography (PET) image reconstruction or radiation therapy planning [4]. These observations indicate a common dilemma when a specific modality is necessary but not possible to obtain in reality. A system, therefore, capable of synthesizing images of interest from several sources, such as different acquisition techniques, and diverse image modalities might be highly advantageous. It can offer the much-needed imaging modality or data for specific clinical purposes without the added expense or risk of conducting an actual acquisition. However, these types of cross-modality medical image-based translation or synthesis is much difficult to directly solve due to the ill-posed and high dimensionality nature of the mapping between the source image and the target image [5], [6], [7], [8].

The quality of images produced by an MRI scanner is mostly determined by the intensity of its magnetic field. MR images in clinical settings are usually obtained with field strengths varying from 0.2T to 3T [3], [9]. However, 7T MRI scanners are increasingly being used in clinical settings following approval from regulatory agencies. A 7T MRI scanner provides superior signal-to-noise ratio (SNR) and spatial resolution compared to a 3T MRI scanner, resulting in enhanced contrast and better anatomical visibility between white matter (WM) and gray matter (GM) tissues, as shown in Figure 2 (a). This enables a more detailed description of cortical folds with subcortical areas, which aids in MRI data analysis processes, such as, anatomical partitioning, tissue segmentation, and reconstructing cortical/subcortical surfaces. It is noted that 3T MR images are inadequate for accurately representing intricate features of anatomical structures and abnormalities. Delineating tiny brain structures like the hippocampus in 3T MRI is challenging due to the restricted spatial resolution [10], [11], [12]. On the other hand, 7T MRI offers superior image quality compared to 3T MRI by exposing specific textural details in the hippocampus. This enhances the ability to observe anatomical structures and improves the application of imaging data. Additionally, 7T MRI has shown clinical effectiveness in detecting minor anomalies caused by pathological diseases [13], [14], [15] that are difficult to identify in low-field MRI. Although beneficial for clinical

studies and research, 7T MRI scanners are not commonly used because of their high cost, complex maintenance, and the expertise needed for image gathering and interpretation [16]. There are approximately 100 7T MRI scanners globally, in contrast to 20,000 3T MRI scanners [17]. Therefore, 7T MRI is costly and not readily available to the general public worldwide. Moreover, this powerful imaging equipment is usually not available to countries with low to moderate income levels. To increase the quality of low-cost MRI, 7T MR images can be generated from the corresponding 3T MRI in order to enhance anatomical details and tissue contrasts, leading to better downstream analysis and processing. However, MRI with low field strength, such as, 0.5T MRI is beneficial for evaluating brain trauma because it reduces susceptibility artifacts and geometric distortions [18], [19]. Thus, 3T MRI might have reduced susceptibility artifacts and geometric distortions compared to 7T MRI, but still 7T MRI is the future of MRI technology. Similar to CT-MRI, translation between 3T MRI and 7T MRI falls under cross-domain image translation as it entails transforming images from one MRI domain (3T MRI) to another (7T MRI), each possessing unique image attributes and quality standards.

The field of MRI has shown substantial progress throughout time, namely in improving the clarity and detail of the images produced. Extensive research and implementation efforts have been dedicated to super-resolution technologies in order to enhance the quality of MRI images. Commonly used techniques encompass interpolation-based methods, learning-based methods, and hybrid methods that integrate several approaches. Nevertheless, recent progress in deep learning, namely in the utilization of Generative Adversarial Networks (GANs), has yielded more resilient solutions.

Previously, multiple studies have made significant contributions to the domain of super-resolution in medical imaging, specifically focusing on endoscopic pictures. The study conducted by Hayat et al. [20] presents a new approach that integrates channel and spatial attention strategies to improve the stereo endoscopic image quality. Another study [21] introduces a network that combines segmentation tasks, and super-resolution, enhancing the usefulness and overall quality of the pictures. The importance of edge guidance in improving video super-resolution, which has potential advantages for real-time applications, has also been highlighted in a recent study [22].

Table 1 presents a concise summary of the benefits, drawbacks, and methodologies used in the current body of research on super-resolution approaches, aiming to offer a thorough understanding of the subject.

GAN models are becoming popular to be utilized for solving tasks such as medical image reconstruction, generation, synthesis, and classification [23], [24]. GAN models, like Deep Convolutional GAN, are mostly utilized to augment datasets [25]. Translation GAN-based models, like cycle consistent GAN (CycleGAN) [26], operate by employing two GAN-based models to produce target images given a

TABLE 1. Recent literatures in the domain of super-resolution methods.

Study	Technique	Advantages	Limitations
Combined Channel and Spatial Attention-based Stereo Endoscopic Image Super-Resolution (2023) [20]	Channel and spatial attention strategies	Improved stereo image resolution and quality	High computational cost, and complex architecture
SEGSNet for Stereo-Endoscopic Image Super-Resolution and Surgical Instrument Segmentation (2024) [21]	Integrated segmentation network and super-resolution	Enhanced segmentation accuracy and improved image quality	Potential for overfitting, requiring extensive training data
E-SEVSR-Edge Guided Stereo Endoscopic Video Super-Resolution (2024) [22]	Edge guidance for video super-resolution	Improved edge preservation and real-time enhancement	High resource requirements, limited to video applications

source image. Generating realistic artificial medical images provides a way to address privacy issues associated with diagnostic imaging and the utilization of people's medical information. Recently, several deep learning techniques for synthesizing images from 3T MRI to 7T MRI have been suggested [1], [17], [27]. A convolutional neural network (CNN) is commonly utilized to develop a non-linear mapping from 3T MRI to 7T MRI, or vice versa, utilizing paired images which must be obtained from the same anatomical locations of the same subjects [28]. Deep learning-based models utilizing adversarial training [1], image priors [27], and cascaded regression [17] have shown the ability to create realistic 7T MR images from the corresponding 3T MRI. However, acquiring paired 3T and 7T MRI for training can be very difficult and challenging in reality. Although CycleGAN-based image translation or synthesis models [26], [29] can be trained without having paired images in the train set, paired data for the test set remain essential for accurate model assessment quantitatively. Furthermore, training CycleGAN with paired data also makes the model more robust by synthesizing target images more accurately [28].

The proposed investigation involves input and output images inside the same MRI domain, however, at different magnetic field strengths, distinguishing it from previous research. Past studies have mostly converted images between different types, for instance, MRI to CT images, or vice versa [1], [2], [28], but have not much focused on converting magnetic field strengths within the same type of paired images. This translation seeks to display MRI at a different anatomical scale. This work aims to assess the capability of cycle consistent generative adversarial deep learning-based methods to convert 3T T1-weighted MRI into a standardized 7T-like MR image quality in order to achieve deep

image harmonization. Deep learning techniques usually need a large number of examples to acquire features that can be applied broadly. However, research on synthesizing images from 3T to 7T is hindered by the limited availability of biomedical imaging data from 7T MRI scanners in clinical sectors. We utilized a trained CycleGAN model to capitalize on a paired 3T-7T MRI dataset. As described earlier, paired 3T – 7T MRI data are mostly unavailable, and very difficult to collect. In the year 2023, Chen et al. [3] published a novel dataset containing paired T1-weighted and T2-weighted brain MRI scans obtained at both 3T and 7T. They also offered a detailed account of the dataset's design, collection, and preparation. Image quality is evaluated utilizing different quality metrics incorporated in the MRI Quality Control (MRIQC) tool [30]. The prime contributions of the present study are delineated as follows.

- The present study is the first one to investigate this paired 3T to 7T and vice versa dataset utilizing CycleGAN models.
- Several experiments have been conducted on the dataset with different architectures of CycleGAN. Each crucial component of CycleGAN has been investigated with the dataset.
- The results of each experiment have been evaluated by several quantitative and qualitative evaluation criteria.
- A post-processing technique has been demonstrated to further increase the accuracy of image generation by CycleGAN.

The present study is organized as follows. Section II demonstrates the methodology of the entire study with discussing all the employed methods, while Section III discusses key findings of the study with critical discussion and comparison. Finally, Section IV concludes the study with stating limitations and future works.

II. METHODOLOGY

The flowchart of the entire study of 3T to 7T MRI conversion, and vice versa using CycleGAN is delineated in Figure 1.

The study commences by preparing and pre-processing the dataset, whereby MRI scans obtained from 3T and 7T sources are gathered, standardized, and supplemented to improve the diversity and quantity of the training dataset. Throughout the training and testing phase, the CycleGAN model undergoes training with different setups of generators, discriminators, and cycle consistency loss functions. The subsequent stage involves analyzing the impact of subject-specific data splitting, which ensures that the data used for training and testing are sourced from distinct subjects in order to assess the model's ability to generalize. Subsequently, we examine the impact of data augmentation strategies on the training set by implementing methods such as rotation, flipping, and scaling to enhance the resilience of the model.

The study also included the goal of predicting 3T MRI from 7T MRI, evaluating the model's ability to translate in both directions. A crucial stage involves the impact of post-processing methods, including skull stripping, to improve

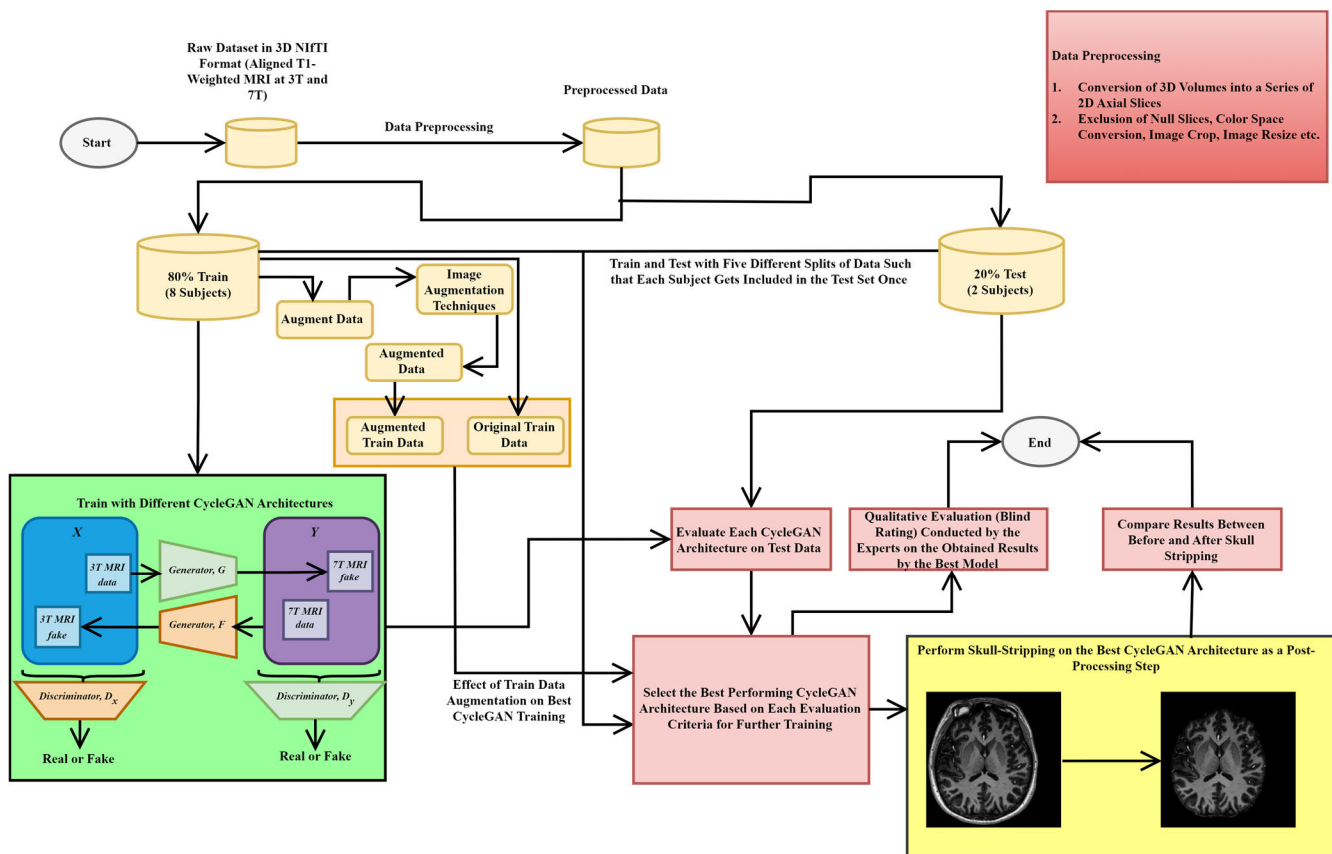


FIGURE 1. The flowchart of the present study on CycleGAN-based MRI translation between 3T and 7T.

the quality of the generated MRIs and make them more suitable for clinical use. In order to validate the suggested method, we conduct a theoretical comparative analysis with established super-resolution methods, emphasizing the differences and benefits of our approach. Subsequently, a thorough examination is conducted to analyze the relative merits of the suggested CycleGAN-based approach in relation to its enhanced adaptability and performance enhancements. Ultimately, a qualitative assessment is performed by expert radiologists to visually evaluate the quality of the translated MRIs. This involves comparing them with ground truth images and the images generated by existing approaches. The displayed flowchart in Figure 1 outlines a comprehensive methodology that guarantees a meticulous assessment and verification of the CycleGAN-based method for translating MRI images between 3T and 7T.

For 3T to 7T MRI translation and vice versa, we have first collected the paired or aligned dataset of T1-weighted 3T and 7T MRI from ten different healthy subjects from a recent publication in the Scientific Data journal [3]. Here, the authors published a dataset containing paired T1-weighted and T2-weighted MRI at 3T and 7T of ten healthy participants to aid in the creation and assessment of 3T-to-7T MR image translation methods. To the best of our knowledge, no previous study has yet experimented with this public dataset for 3T to 7T MRI translation, and vice versa. In the present

study, we have only experimented with axial T1-weighted MRI at 3T and 7T. However, not all MRI slices of each subject in the published dataset possess anatomical information that are beneficial for network training or knowledge extraction. We therefore removed the null slices and kept just the ones with full brain MRI, resulting in around 130 slices per subject. We also excluded the data which are not aligned or paired properly. The selected dataset contains a total of 1297 pairs of slices from 10 subjects (paired 3T and 7T MRI).

Different data preprocessing techniques, such as color space conversion, crop, resize, normalization and others, were employed. All images are standardized to a size of 256×256 pixels. Standardization is essential to maintain constant input size for all images, which helps in batch processing and removes the necessity for dynamic resizing during model training and evaluation. The images' pixel values are normalized by applying a mean and standard deviation of 0.5 to each of the three red, green, and blue (RGB) channels. Normalizing the pixel values to the range of $[-1, 1]$ is a standard procedure for preparing inputs to neural networks. It aids in stabilizing the training procedure by maintaining consistent input magnitude, which can accelerate convergence and enhance the model's generalization capabilities. Consistent with the original article of CycleGAN [26], we have divided the dataset into train and test (external validation) sets.

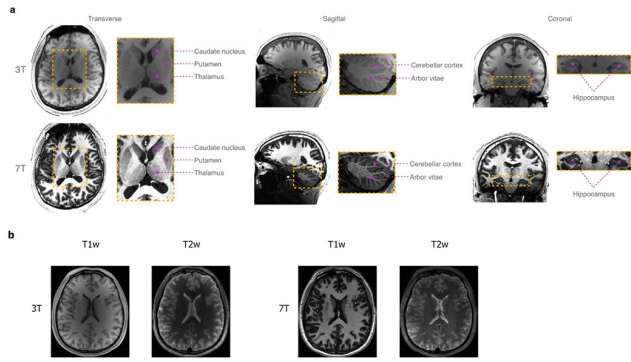


FIGURE 2. Paired T1-weighted (T1w) and T2-weighted (T2w) MRI at 3T and 7T collected from a subject, demonstrated for (a) multiple views, and (b) multiple modalities [3].

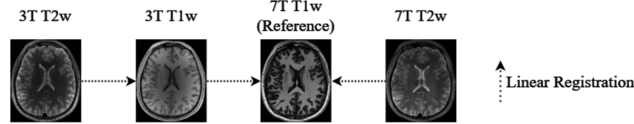


FIGURE 3. Processing of Data: Linear registration of 3T T1-weighted, 3T T2-weighted, and 7T T2-weighted images to 7T T1-weighted image [3].

A. DATASET

Figure 2 delineates few samples from the published article, whereas Figure 3 describes the processing techniques for aligning the MR images to develop a paired dataset of 3T and 7T MRI [3]. Each subject’s 3T T1-weighted and 7T T2-weighted images were aligned with the 7T T1-weighted image using linear registration. The 3T T2-weighted image was aligned with the registered 3T T1-weighted image (Figure 3). More details about data collection and processing techniques can be found in [3].

After selecting the best performing CycleGAN model, we have evaluated the performance of the best model using five different splits of the dataset. For this purpose, we have developed the following five different splits of data (train set and test set) shown in Table 2 based on the selected 1297 pairs of MR images.

TABLE 2. Different train and test datasets used in this study.

Subjects included in the test set	Train set size (Pairs of slices)	Test set size (Pairs of slices)
1, 2	1078	219
3, 4	1026	271
5, 6	1040	257
7, 8	1020	277
9, 10	1024	273

B. CycleGAN ARCHITECTURE

The CycleGAN architecture is our proposed approach to deal with the image translation problem of the present study. We have performed a series of experiments to come up with the best CycleGAN architecture for 3T to 7T MRI conversion, and vice versa, with the highest possible accuracy.

Figure 4 represents the architecture of CycleGAN utilized in this study.

The CycleGAN framework, illustrated in Figure 4, comprises of two primary elements: two generators and two discriminators. The generators are responsible for converting images between the 3T MRI domain and the 7T MRI domain. More precisely, one generator converts 3T MRIs to 7T MRIs, while the second generator carries out the opposite conversion. Both generators employ residual blocks to collect complex characteristics and guarantee precise image reconstruction. The two discriminators have the objective of differentiating between authentic and synthesized images within their individual areas. One discriminator examines the verisimilitude of images in the 3T domain, while the second discriminator appraises the 7T domain. Moreover, the cycle consistency loss guarantees that an image that has been translated from 3T to 7T and then back to 3T (or vice versa) will revert to its original state. This loss is essential for preserving the structural integrity during the translation process. The CycleGAN utilizes adversarial loss and cycle consistency loss to successfully acquire the ability to produce high-quality 7T MRIs from 3T MRIs, while maintaining both intricate details and accuracy.

1) GENERATORS

We have experimented with different architectures of the generator function utilized inside the CycleGAN architecture, which is specifically a Residual Network (ResNet)-based generator. We varied the number of residual layers or blocks employed in the network. The ‘resnet_gen_9’ architecture indicates the ResNet generator consisting of 9 residual blocks which is more complex with higher number of trainable parameters compared to other generators such as, ‘resnet_gen_7’ (ResNet Generator which consists of 7 residual blocks) and ‘resnet_gen_3’ (ResNet Generator which consists of 3 residual blocks). ‘resnet_gen_9’ might be more efficient for more intricate image translation problems when the ability to capture important and significant characteristics is essential. However, it requires more training time and data to avoid convergence and overfitting.

The architecture ‘resnet_gen_7’ is a suitable option for many image translation problems because of its moderate complexity and a potentially lower number of trainable parameters compared to ‘resnet_gen_9’, while still having more parameters than ‘resnet_gen_3’. Therefore, it is anticipated to have a faster speed and necessitates a smaller amount of training data in comparison to ‘resnet_gen_9’.

‘resnet_gen_3’ is the least complex architecture among the three ResNet architectures, while having the fewest trainable parameters. Therefore, it might be suitable for simpler image translation problems where we have limited data. Another advantage is that it is the quickest model in terms of time complexity for model training among the three models, and also less susceptible to overfitting when data is limited.

The ResnetBlock specifies the residual block consisting of two convolution layers. The quantity of these blocks

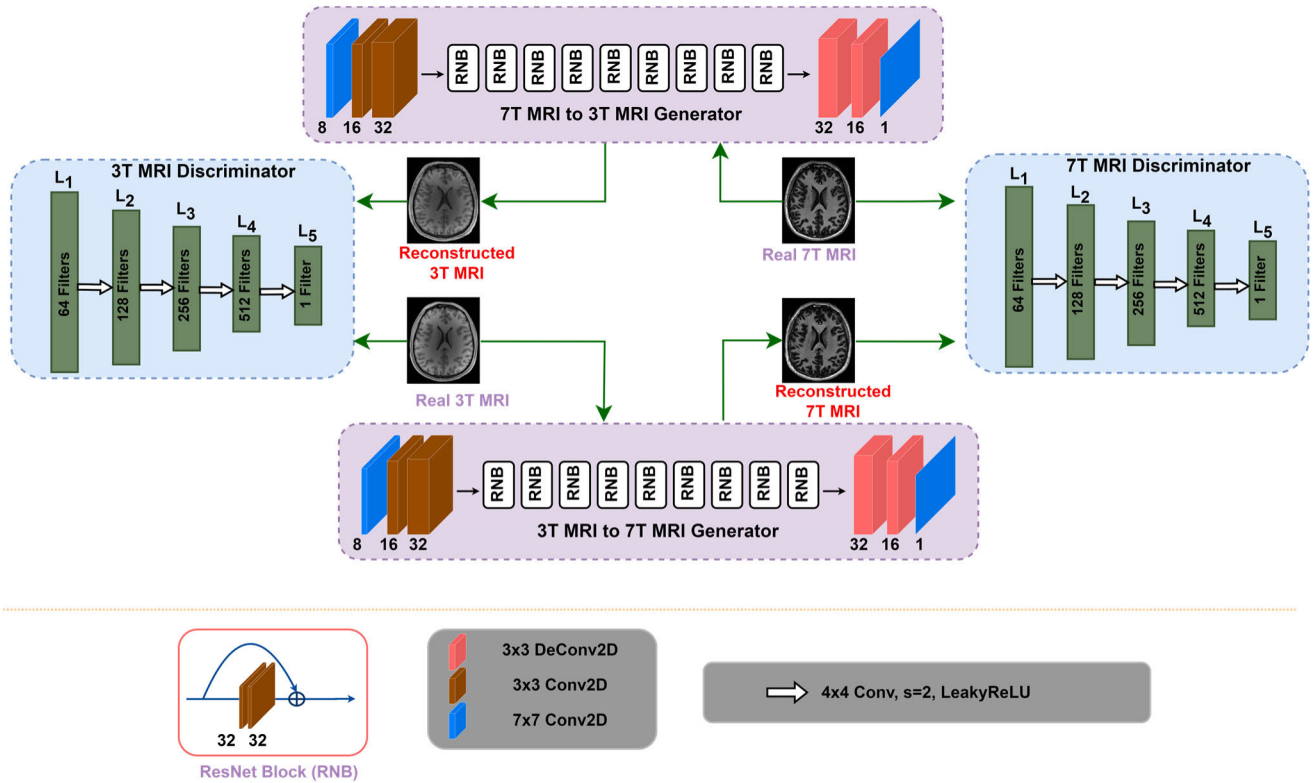


FIGURE 4. The architecture of CycleGAN for the translation between 3T MRI and 7T MRI.

directly affects the model’s ability to comprehend intricate relationships between the input and output domains. A greater number of blocks have the potential to capture more intricate transformations, but this comes at the expense of greater computational complexity.

Each generator variant (‘resnet_gen_9’, ‘resnet_gen_7’, and ‘resnet_gen_3’) adheres to a comparable architectural pattern, mostly varying in the quantity of remaining blocks:

- i. The initial convolution block consists of a solitary convolution layer that utilizes reflection padding and instance normalization.
- ii. The downsampling blocks comprise of a convolution layer, instance normalization, and then rectified linear unit (ReLU) activation, with two such blocks in total. They incrementally increase the number of channels by a factor of two.
- iii. A sequence of residual blocks, with the number of blocks changing (3, 7, or 9) depending on the model variant.
- iv. The upsampling blocks comprise of a transposed convolution layer, instance normalization, and then ReLU activation function. These blocks gradually reduce the number of channels by half.
- v. The final convolution block consists of a solitary convolution layer that utilizes reflection padding, then follows a tan hyperbolic activation function.

2) DISCRIMINATORS

We have further defined two types of discriminator architectures within a CycleGAN model, that are patchGAN and pixelGAN (1×1 patchGAN). Both components play a crucial role in the discrimination process of the GAN, distinguishing between actual and generated images. However, they function based on distinct ideas and scales.

The patchGAN discriminator functions by analyzing patches of the input image. The model employs a sequence of convolutional layers with different strides (kernel size = 4). This architectural design enables the system to concentrate on the texture and style of certain regions within the image, rather than processing the entire image as a whole. The patchGAN model we employ initially consists of 64 channels and progressively augments the number of channels with each subsequent layer (64, 128, 256, 512). The growing intricacy enables it to capture more intricate characteristics at each layer. All convolutional blocks, excluding the first block, incorporate instance normalization technique that normalizes the features for each unique image. The final layer is a convolutional layer that decreases the output to a solitary channel. The resulting dimensions are not limited to 1×1 , but instead provide a compact 2D representation where each cell provides a discrimination score for a corresponding section of the input image.

On the contrary, the pixelGAN discriminator functions at the pixel level by employing 1×1 convolutions. This

implies that it evaluates each individual pixel separately, resulting in a reduced ability to comprehend broader patterns or textures but a heightened emphasis on details at the pixel level. Its architecture consists of a total of three convolutional layers having 1×1 kernels which is much shallower and simpler compared to patchGAN. Instance normalization is only employed in the middle layer. The last layer produces a solitary channel, however, in contrast to patchGAN, its output signifies a discriminating score for every pixel in the image rather than patches.

3) CYCLE CONSISTENCY LOSS FUNCTION

Besides experimenting with different generators and discriminators, we have also experimented with the cycle consistency loss function of the CycleGAN architecture. In the development of the CycleGAN architecture, we utilize both Mean Absolute Error (MAE) and Mean Squared Error (MSE) as metrics for the cycle consistency loss function of the CycleGAN model. These metrics are crucial for ensuring that the generated images accurately reflect the original images, hence maintaining the integrity of the input data throughout the transformation process. The cycle consistency loss is essential for ensuring the model learns bidirectional mappings between domains A (3T MRI) and B (7T MRI). This means that an image translated from domain A to domain B should be able to be translated back to domain A with minimum distortion, and vice versa.

The Mean Absolute Error (MAE) loss ($L1$ loss) is formulated in Equation (1).

$$MAE(G, F) = \frac{1}{N} \sum_{i=1}^N |x_i - G(F(x_i))| + |y_i - F(G(y_i))| \quad (1)$$

In Equation (1), G and F are the generator functions for the translations from domain A (3T MRI) to domain B (7T MRI) and domain B (7T MRI) to domain A (3T MRI), respectively. x_i and y_i represent the images: domain A (3T MRI) and domain B (7T MRI), respectively, with N being the total number of images. This loss metric calculates the average absolute errors between the original images and the corresponding generated images, offering a reliable measure that is resistant to outliers.

On the contrary, the Mean Squared Error (MSE) loss ($L2$ loss) is formulated in Equation (2).

$$MSE(G, F) = \frac{1}{N} \sum_{i=1}^N (x_i - G(F(x_i)))^2 + (y_i - F(G(y_i)))^2 \quad (2)$$

Equation (2) calculates the mean of the squared discrepancies between the original images and the corresponding cycle reconstructions. The MSE loss function gives greater weight to larger errors compared to smaller errors, leading to a more accurate convergence by reducing variance.

The CycleGAN model gains advantages by incorporating both MAE and MSE losses for the cycle consistency loss component, using MAE's resistance to outliers and MSE's

focus on penalizing significant residuals. This dual-loss technique improves the model's capacity to produce high-quality translations that nearly resemble the original data, guaranteeing that the cycle transformation maintains the integrity of the content. By strategically utilizing these losses, our goal is to enhance the performance of the proposed architecture and get improved outcomes in image-to-image translation challenges.

4) FINE-TUNING CycleGAN: OPTIMIZERS, LEARNING DYNAMICS, AND IDENTITY LOSS CONFIGURATION

We have carefully customized the configuration settings in our CycleGAN implementation to enhance the model's performance specifically for image-to-image translation problems. The model functions with a batch size of 1, which is suitable for high-resolution image processing tasks and can work within hardware limitations. Model training consists of two phases: a starting phase of 100 epochs with a constant or linear learning rate, followed by a subsequent 100 epochs with a decaying learning rate (or decay phase), totaling a training period of 200 epochs.

In the context of training a CycleGAN model, an epoch signifies a single iteration over the whole train dataset. Throughout an epoch, the model encounters each example in the entire dataset once. An epoch denotes that the model has tried to translate every unpaired image in the given dataset from domain A (for instance, 3T MRI) to domain B (7T MRI), and vice versa, one time. Epochs represent the frequency at which the learning algorithm's parameters are adjusted using the complete training dataset. The epoch count is a crucial hyperparameter that must be determined before training starts, as it has a significant impact on the model's performance. Insufficient epochs may cause underfitting, whilst excessive epochs might result in overfitting. On the contrary, a checkpoint refers to a preserved state of the model at a specific moment in time while it is being trained. Checkpoints save the precise values of all the parameters (weights and biases) of the model, along with the optimizer state, when saved. This feature enables the training process to be halted and then restarted without any loss of progress. It allows for assessing the model's performance at various points throughout training. Checkpoints are utilized to assess the model's performance at various training phases, aiding in the selection of the most suitable model for a specific task.

The proposed CycleGAN model utilizes MSE loss for both the generator and discriminator, encouraging accurate error reduction by imposing significant penalties for substantial differences between the generated and target images. Another loss function, which is known as the identity loss metric in the CycleGAN model also plays an essential role in maintaining the image content during translation between two different domains. While the cycle consistency loss guarantees minimal loss when translating an image between two domains, the identity loss works on the scenario where an image from domain A (3T MRI) is fed into the generator function that translates the images from domain A (3T MRI)

to A (3T MRI) itself or from domain B (7T MRI) to B (7T MRI). If $G : A \rightarrow B$ and $F : B \rightarrow A$ are the generator functions for the translation of images from domain A (3T MRI) to B (7T MRI) and domain B (7T MRI) to A (3T MRI) respectively, then the identity loss for the generator function, G is defined as the distinction between y and $G(y)$, where y is an image from domain B (7T MRI). Similarly, for the generator function F , the identity loss is formulated as the difference between x and $F(x)$, where x is an image from domain A (3T MRI). The identity loss can be formulated in Equation (3).

$$L_{identity} = \frac{1}{N} \sum_{i=1}^N (|G(y_i) - y_i| + |F(x_i) - x_i|) \quad (3)$$

The identity loss prompts the generator to act as an identity function when given an image from the target domain as input, ensuring little alteration to the image. Integrating identity loss into CycleGAN serves multiple purposes: maintaining content, enhancing stability, and improving quality. The identity loss of CycleGAN is configured as MAE loss in our proposed architecture [26], which enhances resilience to outliers and guarantees that the identity mapping reduces absolute discrepancies.

Both the generator and discriminator are optimized utilizing the Adaptive Moment Estimation (ADAM) optimizer along with a learning rate of $2e-4$ for each, to achieve an efficient and balanced reduction of the utilized loss functions. The design includes a model saving frequency after every 5 epochs, allowing for frequent checkpointing to evaluate and recover the model. Our CycleGAN model is optimized to produce high-quality image translations with strong and coherent training dynamics.

C. DATA AUGMENTATION TECHNIQUES

We also utilized different data augmentation techniques to examine the effect of data augmentation to further improve the performance of image synthesis or reconstruction by the CycleGAN model [31]. Typically, train data augmentation approach mitigates the risk of overfitting by enhancing the diversity of the train dataset. In particular, we have utilized rotation (at 90, 180, and 270 degrees), horizontal flip and vertical flip methods for image augmentation. After employing these data augmentation techniques, the augmented train set contains a total of 6468 pairs of paired 3T-7T MRI.

D. QUANTITATIVE AND QUALITATIVE EVALUATION METRICS

We have utilized different quantitative evaluation metrics, such as, structural similarity index measure (SSIM) [32], peak signal-to-noise ratio (PSNR) [33], normalized mean squared error (NMSE) [34], and normalized mean absolute error (NMAE) [35], which are the most widely used evaluation criteria for most of the previous image-to-image translation-based tasks. Furthermore, we relied on expert validation by doctors and radiologists, which could be categorized as a pure qualitative evaluation criterion [36], which is considered

even more important compared to the quantitative metrics for these types of problems. These evaluation metrics are typically utilized to assess the performance of various image processing and signal processing tasks. The mathematical equations for each metric utilized in this study are described as follows.

SSIM mainly quantifies the resemblance between two images. SSIM is defined in Equation (4).

$$SSIM(x, y) = \frac{(2\mu_x\mu_y + c_1)(2\sigma_{xy} + c_2)}{(\mu_x^2 + \mu_y^2 + c_1)(\sigma_x^2 + \sigma_y^2 + c_2)} \quad (4)$$

In Equation (4), x and y denote the two images to be compared. μ_x and μ_y indicate the average intensities of images x and y . σ_x^2 and σ_y^2 denote the variances of these two images. σ_{xy} refers to the covariance between these two images. c_1 and c_2 are constants used to stabilize the division operation when the denominator is weak, the following Equation (5) is typically considered.

$$c_1 = (k_1L)^2 \text{ and } c_2 = (k_2L)^2 \quad (5)$$

In Equation (5), L represents the dynamic range of pixel values, typically 255 for 8-bit pictures. By default, k_1 is taken as 0.01, whereas k_2 is taken as 0.03.

PSNR is mostly utilized to assess the quality of reconstruction in lossy compression codecs. PSNR is defined in Equation (6).

$$PSNR = 10 \log_{10} \left(\frac{MAX_I^2}{MSE} \right) \quad (6)$$

In Equation (6), MAX_I indicates the maximum pixel value of the image (for instance, 255 for 8-bit images). MSE refers to the mean squared error between the original and compressed or reconstructed image.

NMSE is a standardized form of the mean squared error (MSE) commonly employed to assess the likeness between two images. NMSE is defined in Equation (7).

$$NMSE = \frac{\sum_{i=1}^N (x_i - y_i)^2}{\sum_{i=1}^N x_i^2} \quad (7)$$

In Equation (7), x_i and y_i refer to the pixel values of the original and predicted images, respectively. N indicates the total number of pixels in each image.

NMAE is an alternative way to normalize the mean absolute error (MAE), offering a scale-independent metric for error assessment. NMAE is defined in Equation (8).

$$NMAE = \frac{\sum_{i=1}^N |x_i - y_i|}{\sum_{i=1}^N |x_i|} \quad (8)$$

In Equation (8), x_i and y_i denote the pixel values of the original and predicted images, respectively. N refers to the total number of pixels in each image.

All these quantitative metrics offer different viewpoints on the quality and precision of image reconstruction or synthesis algorithms, considering factors such as structural integrity, error magnitude and noise etc. However, qualitative assessment is also crucial for synthesizing MR images between

3T and 7T as it considers subjective elements like perceptual clarity and diagnostic utility, which are vital in medical imaging but may not be completely measured by numerical metrics. Human specialists can evaluate subtle differences in image contrast, texture, and anatomical detail crucial for precise diagnosis, which quantitative measurements may not capture accurately in terms of clinical significance.

Therefore, we performed a detailed qualitative assessment on the utility and fidelity of MR images translated between magnetic field strength of 3T and 7T using CycleGAN. This qualitative evaluation turns out to be essential for comprehending the technical capacities of the proposed CycleGAN architecture as well as its possible use in therapeutic settings. Three experienced radiologists from Hamad Medical Corporation, Qatar, were included in a no-reference evaluation process to guarantee the quality and relevance of our findings. Each expert received a dataset of 20 3T MRI and 20 7T MRI scans. The dataset was meticulously selected from an external validation set with 219 slices from two different subjects to ensure a varied representation of anatomical characteristics and pathologies. These external validation images were chosen based on particular criteria to provide a wide range of challenges to the CycleGAN model, ensuring a thorough evaluation of its performance in various settings.

The image selection approach was systematic, rigorous, and randomized. The inclusion criteria were established to guarantee that the chosen MR images included a wide variety of anatomical components, including both normal and diseased appearances, in order to evaluate the model's performance in diverse clinical situations. Exclusion criteria were used to eliminate MR images with severe motion artifacts or inadequate contrast that could unfairly impact the qualitative rating. The selection technique entailed randomly selecting 20 MR images from every modality (3T MRI and 7T MRI) out of a total of 219 images of each modality, with each image having an equal probability of being selected. The randomization was conducted by a straightforward random sampling method to ensure an unbiased and representative selection of images for assessment. Here, each image i in the external validation dataset of N MR images was given a distinct identifier. A random number generator was then utilized to choose n images without repetition, with n being equal to 20. Equation (9) delineates the formula for this process.

$$S = \{s_i | s_i \in N \text{ and } |S| = n\} \quad (9)$$

In equation (9), S represents the set of chosen samples, s_i is a chosen image, N is the entire set of images, and n is the number of images to be chosen.

During the no-reference evaluation process, 20 authentic or real images were intermingled with 20 fake or CycleGAN-generated images in such a way that obscured their actual origin from the assessors. Anonymized filenames were used along with a random sequence generator to establish the order of image presentation. This technique prevented the evaluators from deducing if an image was real

or CycleGAN-generated depending on its location in the sequence.

The evaluation criteria were meticulously selected to mirror crucial features for the clinical usefulness and technological achievement of the utilized CycleGAN model. The images were qualitatively evaluated on a Likert scale from 1 to 10 based on three criteria: Image Quality (evaluating contrast, sharpness, artifact presence and noise level), Diagnostic Utility (assessing the usefulness of the images for clinical diagnoses or recognizing pathologies), and Realism (quantifying resemblance to authentic MR images in terms of anatomical accuracy and texture). The Likert scale method enabled a detailed evaluation of the MR images, which allowed for a thorough examination of the actual performance of the model.

Ethical issues and confidentiality were of utmost importance during this study. The evaluated images were obtained from a recent publication in the Scientific Data journal [3] and adhered to all applicable ethical norms. Before usage, all the images were de-identified to protect the confidentiality and privacy of the subjects. This study is committed to upholding the highest standards of integrity through adherence to ethical norms.

E. HARDWARE, SOFTWARE AND TOOLS

We utilized a wide range of software libraries and tools based on PyTorch and PyTorch Lightning, to aid in developing, training, and testing our CycleGAN model in this study. For the training of CycleGAN, we have utilized NVIDIA GeForce RTX 4090 GPU with a video random access memory (VRAM) of 24GB. For skull stripping in MRI, we have used the polygonal region of interest, *roipoly* function in MATLAB R2022a software.

III. RESULTS AND DISCUSSION

To conduct a thorough and rigorous investigation, we have performed a total of 40 experiments at different checkpoints (spanning from epoch 5 to epoch 200, with an interval of 5 epochs) for each CycleGAN architecture. To find the best model, we have used the first two subjects' data for testing (subject 1 and 2) and the remaining eight subjects' data for training (subject 3 – 10). Thus, the train set contains a total of 1078 pairs of train MR images (paired 3T and 7T) from 8 different subjects, whereas the test set contains 219 pairs of paired images from 2 subjects.

Based on all the stated quantitative and qualitative evaluation criteria altogether, we have selected the best epoch for each CycleGAN architecture and finally the best CycleGAN architecture among all the architectures under investigation for solving this task. Table 3 describes the summary of all the results for 3T to 7T MRI translation among five different CycleGAN architectures based on different generators, discriminators, and cycle consistency loss functions.

Table 3 displays a comprehensive comparison of multiple CycleGAN-based models assessed for the 3T to 7T MRI translation task, emphasizing their performance metrics

TABLE 3. Summary of different CycleGAN-based results for 3T TO 7T MRI translation.

Model Name	Best SSIM	Best PSNR (dB)	Best NMSE	Best NMAE
resnetgen9_patchGAN_MAE	69.22% (Epoch 80)	18.23 (Epoch 65)	0.0155 (Epoch 80)	0.2166 (Epoch 100)
resnetgen9_patchGAN_MSE	70.88% (Epoch 130)	19.15 (Epoch 175)	0.0129 (Epoch 175)	0.2297 (Epoch 115)
resnetgen7_patchGAN_MSE	68.60% (Epoch 200)	18.26 (Epoch 45)	0.0155 (Epoch 45)	0.2164 (Epoch 180)
resnetgen3_patchGAN_MSE	70.73% (Epoch 125)	18.80 (Epoch 175)	0.0139 (Epoch 175)	0.1916 (Epoch 180)
resnetgen9_pixelGAN_MSE	66.33% (Epoch 5)	16.50 (Epoch 10)	0.0229 (Epoch 10)	0.2260 (Epoch 25)

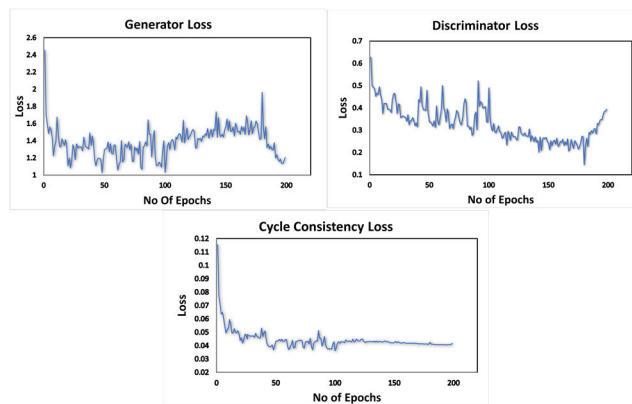
under varied settings. The models are categorized according to the generator type (resnetgen3, resnetgen7, resnetgen9), discriminator type (patchGAN, pixelGAN), and the loss function used for cycle consistency (MAE, MSE). The table presents the highest attained values of the SSIM, PSNR, NMSE, and NMAE for each model, along with the number of training epochs associated with each value. The resnetgen9_patchGAN_MSE model attained a peak SSIM of 70.88% during epoch 130, demonstrating its superior structural resemblance to the ground truth. The model achieved the highest PSNR of 19.15 dB at epoch 175, indicating outstanding image clarity and noise reduction. The resnetgen9_patchGAN_MSE model achieved the lowest NMSE of 0.0129 at epoch 175, indicating high reconstruction accuracy. On the other hand, the resnetgen3_patchGAN_MSE model achieved the best NMAE of 0.1916 at epoch 180.

Additionally, other models exhibited noteworthy performance, albeit with minor discrepancies. The resnetgen9_patchGAN_MAE model demonstrated an SSIM of 69.22% at epoch 80 and a PSNR of 18.23 dB at epoch 65. These results indicate a well-balanced performance, but not as high as the MSE variant. The resnetgen7_patchGAN_MSE model achieved an SSIM of 68.60% at epoch 200 and a PSNR of 18.26 dB at epoch 45. These findings suggest that the model performs well, but further modification might be needed to get ideal outcomes. The resnetgen9_pixelGAN_MSE model, despite yielding an SSIM of 66.33% at epoch 5 and a PSNR of 16.50 dB at epoch 10, offered useful insights into the influence of various discriminators.

Regarding ranking, the resnetgen9_patchGAN_MSE model consistently beat other models, with the resnetgen3_patchGAN_MSE model following closely behind, demonstrating strong performance and achieving the best NMAE. The models resnetgen9_patchGAN_MAE and resnetgen7_patchGAN_MSE exhibited balanced performance metrics, albeit somewhat lower. On the other hand,

the resnetgen9_pixelGAN_MSE model yielded the least favorable results, emphasizing the significance of selecting an appropriate discriminator. The table presents information on the trade-offs and performance variations among various model settings, highlighting the resilience and efficacy of the resnetgen9_patchGAN_MSE model in generating high-quality MRI translations.

Among all the employed architectures shown in Table 3, the resnetgen9_patchGAN_MSE model performed best based on all the quantitative and qualitative evaluation criteria altogether. Furthermore, according to the radiologists, epoch 130 (having the best SSIM score) of the resnetgen9_patchGAN_MSE model turns out to produce the best generated 7T MR images. In Table 3, the best architecture is highlighted in boldface whereas the best epoch (according to the radiologists) is highlighted in boldface green. Figure 5 illustrates the change in loss across epochs for the generator, discriminator, and cycle consistency loss function of the top-performing resnetgen9_patchGAN_MSE architecture.

**FIGURE 5.** Variation of loss over the progression of epochs for the generator, discriminator, and cycle consistency loss function of the best performing resnetgen9_patchGAN_MSE architecture.

The generator loss signifies the improvement of the generator in generating high-resolution images that are more realistic as the training advances through many epochs. The discriminator loss exhibits considerable fluctuations during the first learning phase as it endeavors to differentiate between authentic and synthesized images. Over time, the discriminator loss reaches a state, indicating a balanced adversarial training state where the generator and the discriminator do not have an overwhelming advantage individually. The cycle consistency loss exhibits a consistent decrease, indicating the enhanced capability of the model to preserve the structural integrity of the generated images. The decrease in cycle consistency loss is essential as it guarantees that the generated images maintain fidelity to the original 3T MRI images while attaining the targeted 7T resolution.

A. ABLATION STUDY

An ablation study assesses the effectiveness of an artificial intelligence (AI) system by methodically eliminating certain

components. This method aids in comprehending the individual impact of each component on the overall efficiency of the AI system. In this subsection, we performed an ablation study based on different generators, discriminators, and cycle consistency loss functions of CycleGAN model for 3T to 7T MRI translation based on the results derived from Table 2.

1) COMPARISON AMONG GENERATORS (RESNETGEN3 VS RESNETGEN7 VS RESNETGEN9)

Comparing different CycleGAN models using distinct generators (resnetgen3, resnetgen7, and resnetgen9) for translating MRI images from 3T to 7T shows notable differences in performance based on SSIM, PSNR, NMSE, and NMAE metrics. The CycleGAN models based on resnetgen9 generator, utilizing MAE and MSE loss functions as the cycle consistency loss, exhibit higher SSIM and PSNR values than the resnetgen3 and resnetgen7-based CycleGAN models, suggesting improved signal-to-noise ratio and structural similarity which are important for maintaining fidelity in medical imaging. The resnetgen9 model, trained using Mean Squared Error (MSE) cycle consistency loss function, particularly excels with an SSIM of 70.88% and a PSNR of around 19.15, indicating its superior capacity to capture and process intricate structures in MR images. On the contrary, the resnetgen3-based model demonstrates a competitive SSIM of 70.73%, almost similar to the resnetgen9-MSE model, however, with a slightly larger NMSE and the least NMAE. This suggests a delicate balance between preserving detailed structure and minimizing overall error. The resnetgen7-based model demonstrates balanced performance across various metrics, indicating that while the more complex resnetgen9-based model has its benefits, the efficiency of resnetgen3 in specific metrics underscores the significance of selecting a model depending on specific performance objectives.

2) COMPARISON AMONG DISCRIMINATORS (patchGAN VS pixelGAN)

The function of the discriminator in CycleGAN frameworks, when comparing patchGAN with pixelGAN, emphasizes how the granularity of the discriminator affects the quality of translating 3T to 7T MR images. The patchGAN discriminators, when combined with resnetgen3, resnetgen7, and resnetgen9-based generators, consistently outperform the pixelGAN-based discriminator in terms of PSNR and SSIM across all architectures. The patchGAN discriminators help to improve structural similarities and image quality, as shown by their better SSIM and PSNR metrics. The pixelGAN model's emphasis on pixel-level differences, as indicated by its SSIM of 66.33% and PSNR of 16.50, which is significantly lower compared to the performance of the other models, may be advantageous for capturing intricate details but might not be as successful in maintaining the overall structure and reducing noise in MRI translation. This comparative study signifies the necessity of selecting a discriminator that agrees with the important characteristics of image quality related to the task.

3) COMPARISON AMONG CYCLE CONSISTENCY LOSS FUNCTIONS (MAE VS MSE)

The selection of the cycle consistency loss function, particularly between MAE and MSE losses, significantly impacts the performance of CycleGAN models for MR image conversion. The resnetgen9-based model with MSE cycle consistency loss performs better compared to its MAE counterpart in the SSIM metric with scores of 70.88% and 69.22% respectively, suggesting somewhat superior structural preservation. MSE's sensitivity to greater errors may be more beneficial for capturing intricate structural information in MR images, which is crucial for medical diagnosis and assessment. The MAE loss, albeit somewhat behind in SSIM, demonstrates similar performance in metrics like PSNR and NMSE, suggesting its overall strength in preserving image quality. The decision to use either MAE or MSE cycle consistency loss functions depends on the particular needs of the translation problem. MSE may be slightly more beneficial for tasks that prioritize structural accuracy, while MAE is better suited for general image translation problems that aim for balanced performance across different quality metrics.

B. EFFECT OF SUBJECT – SPECIFIC DATA SPLITTING INTO TRAIN AND TEST SETS

We further analyzed the performance of the best performing resnetgen9_patchGAN_MSE-based CycleGAN model by testing it on different test splits of the dataset. Table 4 reports the performance of the model based on each quantitative evaluation criterion on five different test (external validation) datasets, each containing data from distinct subjects. Analyzing the model's performance on these datasets shows important patterns and fluctuations in SSIM, PSNR, NMSE, and NMAE, which are essential for evaluating 3T to 7T MRI conversion quality.

TABLE 4. Performance of the resnetgen9_patchGAN_MSE model on different test sets.

Test Set	Best SSIM	Best PSNR (dB)	Best NMSE	Best NMAE
Subject 1, 2	70.88% (Epoch 130)	19.15 (Epoch 175)	0.0129 (Epoch 175)	0.2297 (Epoch 115)
Subject 3, 4	69.58% (Epoch 50)	18.53 (Epoch 70)	0.0152 (Epoch 70)	0.2388 (Epoch 170)
Subject 5, 6	69.05% (Epoch 120)	17.51 (Epoch 105)	0.0192 (Epoch 105)	0.2988 (Epoch 170)
Subject 7, 8	68.07% (Epoch 20)	19.19 (Epoch 110)	0.0125 (Epoch 110)	0.2292 (Epoch 190)
Subject 9, 10	70.11% (Epoch 110)	18.68 (Epoch 195)	0.0145 (Epoch 195)	0.1760 (Epoch 145)

The average SSIM for each test set is 69.54% (standard deviation: 0.95), suggesting a consistent capability of the model to maintain structural features among various subjects. The PSNR metric has an average value of 18.61

(standard deviation: 0.61), indicating a minor variation in the model’s capacity to reduce noise while preserving signal quality. The NMSE and NMAE metrics have mean values of 0.0149 and 0.2345, respectively. NMSE has a standard deviation of 0.00239, indicating slightly more variability compared to NMAE, which has a standard deviation of 0.03905. This suggests variations in the model’s accuracy in predicting pixel values among different subjects.

The variance in these metrics, particularly the higher variance in SSIM and NMAE metrics, highlights the model’s varying sensitivity to the distinct physiological and anatomical features presented in the MRI data of each subject. The model performed best in terms of SSIM on the test sets of Subject 1, 2 and Subject 9, 10, indicating its effectiveness in the translation of MR images with similar structural properties. Conversely, the test dataset with subject 7 and 8 exhibits the greatest PSNR, showcasing outstanding noise reduction ability in this specific test set. The subjects with the lowest NMSE are 7 and 8, while the subjects with the lowest NMAE are 9 and 10. This highlights the varying effectiveness of the model among different participants.

This detailed assessment demonstrates the intricate performance of the resnetgen9_patchGAN_MSE model in the task of translating MR images from 3T to 7T. The results indicate that the model’s accuracy and quality are generally excellent but can vary slightly based on the individual properties of the MRI data being converted. The insights enhance our comprehension of the model’s capacities and emphasize the significance of taking subject variability into account when developing and evaluating CycleGAN-based medical image synthesis systems.

Figure 6 shows few results generated by the best performing model (resnetgen9_patchGAN_MSE: Epoch 130) on each test (external validation) set along with the corresponding ground truth and input images.

C. EFFECT OF DATA AUGMENTATION TECHNIQUES ON TRAIN SET

We further experimented with the resnetgen9_patchGAN_MSE model to examine its performance after training it with the augmented train dataset consisting of a total of 6468 pairs of paired 3T – 7T MR images. In other words, we assessed the effect of train data augmentation techniques on the best performing model using subject 1 and 2 as the external validation dataset. Table 5 delineates the quantitative results before and after applying train data augmentation techniques.

As can be observed from Table 5, train data augmentation raised SSIM by a little margin. However, the PSNR decreased while we noticed almost no difference in NMSE. Lastly, applying train data augmentation techniques significantly lowered the NMAE on the test set. Figure 7 shows few results generated by the CycleGAN model both before and after augmentation along with the corresponding ground truth and input images.

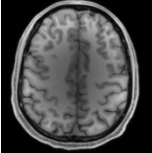
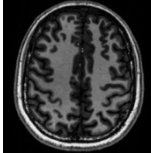
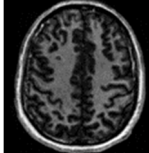
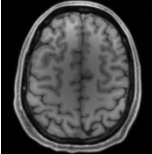
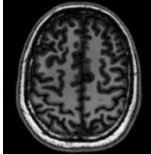
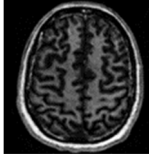
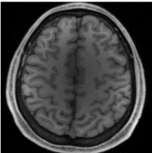
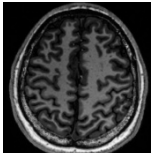
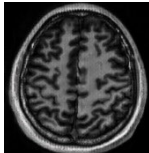
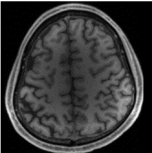
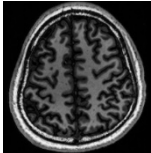
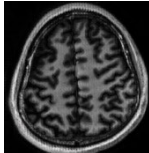
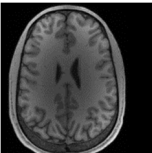
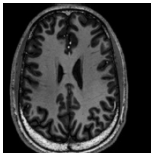

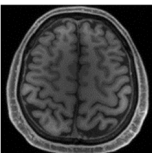
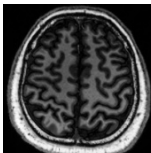
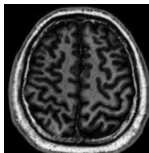
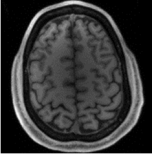
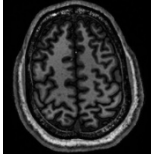
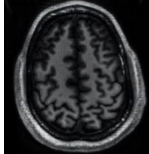
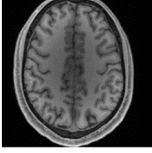
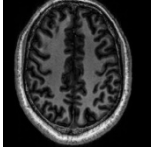

Test Set (Based on Subjects)	Input 3T MRI	Ground Truth 7T MRI	Predicted 7T MRI
Subject 1 and 2			
Subject 1 and 2			
Subject 3 and 4			
Subject 3 and 4			
Subject 5 and 6			
Subject 5 and 6			
Subject 7 and 8			
Subject 7 and 8			

FIGURE 6. 7T MRI generated from 3T MRI on each test set by the resnetgen9_patchGAN_MSE model.

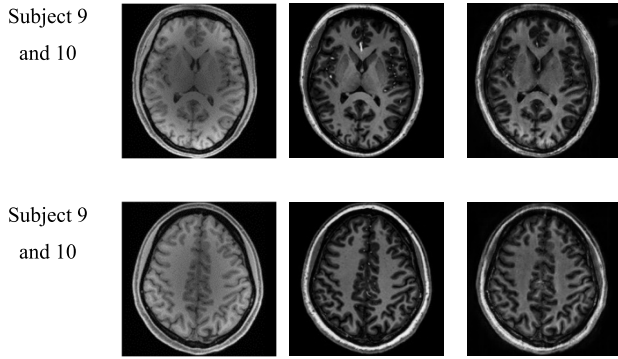


FIGURE 6. (Continued.) 7T MRI generated from 3T MRI on each test set by the resnetgen9_patchGAN_MSE model.

According to the qualitative comments given by all the three experts, the predicted MR images (especially the white region of the brain) turn out to be better with the model before applying any train data augmentation techniques, whereas the predicted MR images appear to contain dark artifacts after exploiting the train data augmentation processes. Thus, 3T MRI to 7T MRI prediction turns out to be better when we did not augment the train dataset for CycleGAN training as per the qualitative validation conducted by all the experts, although quantitatively, augmentation techniques performed better in terms of SSIM and NMAE (Table 5).

TABLE 5. Effect of train data augmentation ON 3T MRI TO 7T MRI conversion by the resnetgen9_patchGAN_MSE model.

Model Name	Best SSIM	Best PSNR (dB)	Best NMSE	Best NMAE
resnetgen9_patchGAN_MSE (without train data augmentation)	70.88% (Epoch 130)	19.15 (Epoch 175)	0.0129 (Epoch 175)	0.2297 (Epoch 115)
resnetgen9_patchGAN_MSE (after train data augmentation)	71.07% (Epoch 45)	18.62 (Epoch 45)	0.0145 (Epoch 45)	0.1869 (Epoch 50)

D. 3T MRI PREDICTION FROM 7T MRI

We have utilized the resnetgen9_patchGAN_MSE-based CycleGAN model for the task of 7T to 3T MRI translation and the results are demonstrated in Table 6.

Unlike 3T to 7T MRI translation, the model with the best NMSE metric (highlighted in boldface in Table 6) generated more realistic images with respect to the ground truth images compared to the model with the best SSIM metric for 3T MRI prediction from 7T MRI, according to the qualitative evaluation conducted by all the experts. Figure 8 shows few results of 7T to 3T MRI conversion by the best model with the least NMSE metric (Epoch 175).

The main objective of this study is to use CycleGAN to convert 3T MRI to 7T MRI. This direction is of great clinical importance and has the potential to enhance diagnostic imaging. Although CycleGAN naturally allows for bidirectional translation, our main focus was not on the 7T to 3T conversion. Therefore, we only included a brief mention of it. The

TABLE 6. Summary of results of the resnetgen9_patchGAN_MSE model for 7T TO 3T MRI conversion.

Model Name	Best SSIM	Best PSNR (dB)	Best NMSE	Best NMAE
resnetgen9_patchGAN_MSE	74.50% (Epoch 85)	21.02 (Epoch 165)	0.0080 (Epoch 175)	0.2619 (Epoch 170)

versatility of CycleGAN’s architecture enables it to effectively process diverse image kinds, including color images. CycleGAN has demonstrated excellent applications in various fields, particularly in challenges related to color picture translation. For instance, it has been used effectively to convert photographs into different artistic styles or to improve the resolution of natural images [26]. These applications showcase the model’s versatility and resilience across several picture categories, highlighting the potential of CycleGAN for addressing a wide range of imaging challenges beyond grayscale MRI.

E. EFFECT OF POST-PROCESSING TECHNIQUE: SKULL STRIPPING

It is also noted that we have performed a post processing technique, skull stripping in MRI [37], to achieve better results on image translation. Skull stripping is a technique employed in medical imaging to segregate the brain tissue from the other components of the image, such as the scalp, skull, and other non-brain structures. It is a crucial procedure in the processing of brain MRI, which allows for a more targeted and precise study of brain tissue. This method is essential for various brain analyses and diagnostics. Through the elimination of non-brain components, doctors can enhance their emphasis on brain tissue with more precision, which is a crucial aspect in automated analyses and deep learning applications. Skull stripping is a crucial first step to achieve optimal results in different neuroimaging tasks [37].

Table 7 delineates the effect of skull stripping on 3T MRI to 7T MRI conversion, and vice versa.

Skull stripping as a post-processing strategy significantly improves image quality metrics when converting 3T MRI to 7T MRI using a CycleGAN architecture with the resnetgen9_patchGAN_MSE model. Table 7 shows that using skull stripping as a post-processing method improves the SSIM from 70.88% to 83.80% and PSNR from 18.83 to 26.25. Additionally, there is a significant decrease in the NMSE from 0.0139 to 0.0088, and the NMAE drops from 0.2906 to 0.0630. These findings suggest that excluding irrelevant anatomical components like the skull considerably improves the model’s capacity to effectively convert 3T MR images to higher resolution 7T MR images, enhancing both structural accuracy and overall image quality.

Conversely, the effect of skull stripping on converting 7T MRI to 3T MRI, as shown in Table 7, again demonstrates significant enhancements in the quality of the generated images. Pre-skull stripping, the SSIM and PSNR metric values are 73.64% and 21.02, respectively. However, post-skull

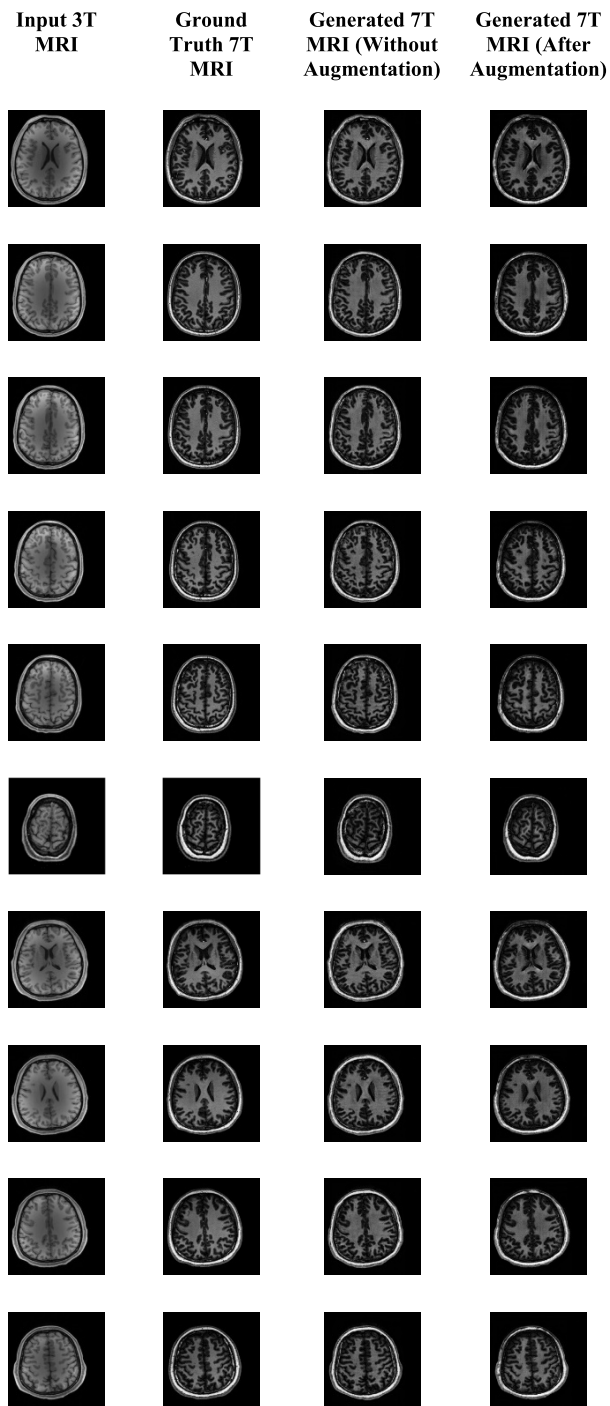


FIGURE 7. Effect of train data augmentation techniques on the resnetgen9_patchGAN_MSE model.

stripping, these values improve to 85.81% and 25.07, respectively. Furthermore, the NMSE and NMAE measures have significantly improved, with NMSE decreasing from 0.0080 to 0.0036, and NMAE dropping from 0.2883 to 0.1076. These improvements highlight the importance of skull stripping in enhancing the image quality and translation accuracy while translating from 7T MRI to 3T MRI. The decrease in residuals and improvement in similarity measures after skull stripping demonstrate its effectiveness in isolating

TABLE 7. Effect of skull stripping as a post-processing technique on 3T MRI to 7T MRI conversion (EPOCH 130) and 7T MRI TO 3T MRI conversion (EPOCH 175).

Task	Model Name	Best SSIM	Best PSNR (dB)	Best NMSE	Best NMAE
3T MRI to 7T MRI	resnetgen9_patchGAN_MSE (Before skull stripping)	70.88%	18.83	0.0139	0.2906
	resnetgen9_patchGAN_MSE (After skull stripping)	83.80%	26.25	0.0088	0.0630
7T MRI to 3T MRI	resnetgen9_patchGAN_MSE (Before skull stripping)	73.64%	21.02	0.0080	0.2883
7T MRI to 3T MRI	resnetgen9_patchGAN_MSE (After skull stripping)	85.81%	25.07	0.0036	0.1076

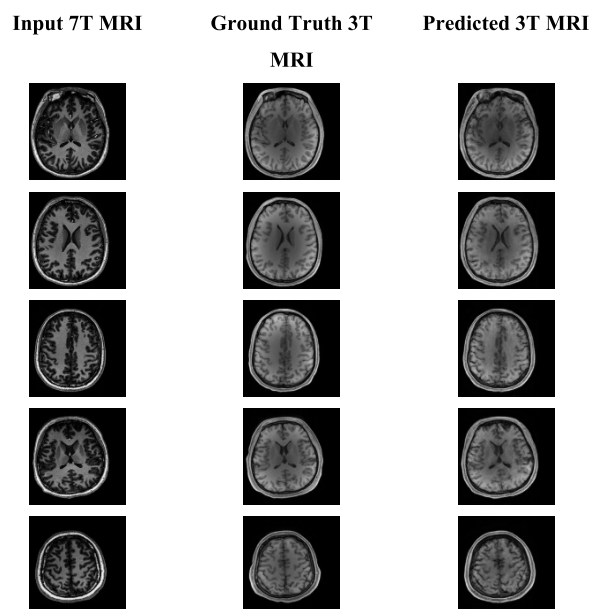


FIGURE 8. 7T MRI to 3T MRI translation using the best performing CycleGAN model.

the essential diagnostic features required for precise MRI interpretation, thus confirming the importance of skull stripping as a beneficial post-processing stage in improving the efficiency of CycleGAN-based MRI synthesis models.

Figure 9 shows few results generated by the best model, resnetgen9_patchGAN_MSE (Epoch 130) for 3T to 7T MRI translation, both before and after skull stripping.

Figure 10 shows few results generated by the best model, resnetgen9_patchGAN_MSE (Epoch 175) for 7T to 3T MRI translation, both before and after skull stripping.

F. COMPARATIVE ANALYSIS WITH EXISTING SUPER-RESOLUTION METHODS

In order to evaluate the potential efficacy of our strategy, which is based on CycleGAN model, for translating 3T to 7T MRI images, we conducted a theoretical comparison with

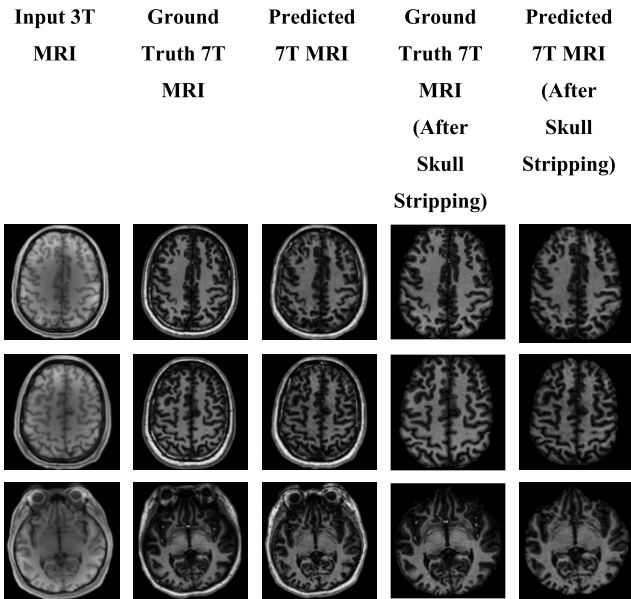


FIGURE 9. Predicted results by the best CycleGAN model for 3T to 7T MRI translation (before and after skull stripping).

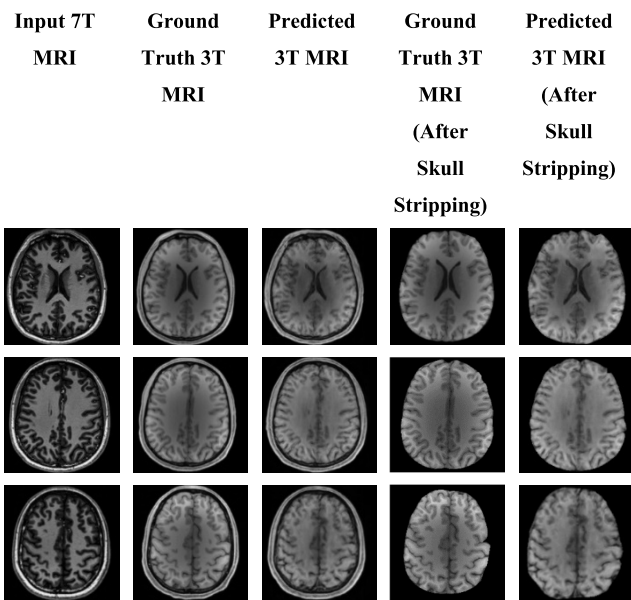


FIGURE 10. Predicted results by the best CycleGAN model for 7T to 3T MRI translation (before and after skull stripping).

established super-resolution techniques. Conventional interpolation techniques, such as, bicubic and nearest-neighbor interpolation, are frequently criticized for their failure to maintain fine details and their vulnerability to artifacts. Learning-based approaches, such as deep CNNs, show substantial advancements but present difficulties such as the requirement for abundant training data and substantial computer resources.

The approach we propose involves using a CycleGAN model with varying generators (resnetgen3, resnetgen7, and resnetgen9), discriminators (patchGAN and pixelGAN), and cycle consistency loss functions (MAE and MSE). This

approach is designed and proposed to potentially surpass the traditional and conventional methods by maintaining structural details and reducing artifacts. The intrinsic cycle consistency of CycleGANs guarantees that the generated images preserve the original content, resulting in high-resolution images that are more accurate and realistic.

Although we did not directly compare our CycleGAN-based technique with super-resolution approaches in an experiment, the theoretical advantages of our approach indicate that it has the potential to provide better outcomes in MRI translation. Future study will involve doing empirical validation to confirm the theoretical advantages stated here, in comparison to these conventional methods.

G. COMPARATIVE CONTRIBUTIONS OF THE PROPOSED CYCLEGAN-BASED METHOD

Our suggested CycleGAN-based technique offers substantial contributions in comparison to other relevant technologies. Conventional GAN-based methods have achieved success in many image translation tasks, but they frequently necessitate a substantial quantity of paired training data. Obtaining such data might be difficult in the field of medical imaging. Our approach overcomes this restriction by even utilizing unpaired training data, facilitated by the cycle consistency loss.

Utilizing several generator topologies, such as resnetgen3, resnetgen7, and resnetgen9, provides the ability to adjust the balance between computing efficiency and image quality. The selection of discriminators (patchGAN and pixelGAN) ensures the ability to accurately differentiate between authentic and synthesized images across various levels of detail. In addition, by testing several cycle consistency loss functions, such as, MAE and MSE, we can refine the model to achieve optimal performance and ensure the translation of high-quality images.

To summarize, our CycleGAN-based method for translating 3T to 7T MRI has clear benefits compared to current super-resolution techniques. These advantages include the capacity to handle unpaired data, versatility in architectural design, and enhanced image quality. Our method’s contributions greatly enhance the MRI image resolution for clinical applications, making it a vital addition to the medical image super-resolution domain.

H. QUALITATIVE EVALUATION

Figure 11 represents the average qualitative ratings on a Likert Scale from 1 to 10 (with 1 being the worst and 10 being the best) given by the expert radiologists during the no-reference qualitative evaluation process for the systematically selected twenty fake 3T and 7T MR images generated by the best performing CycleGAN model.

1) AVERAGE QUALITATIVE RATINGS FOR FAKE 3T MR IMAGES

The generated 3T MR images are rated an average of 7.10 out of 10 for image quality. These generated images exhibit

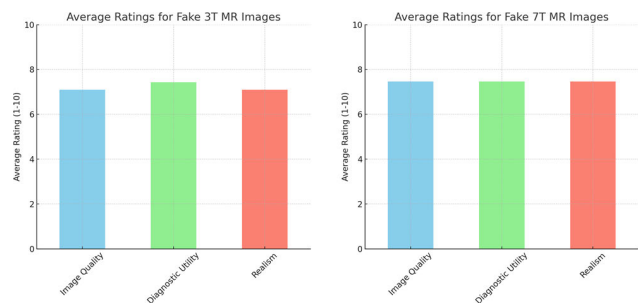


FIGURE 11. Qualitative evaluation conducted by the experts on the generated or fake images based on three different evaluation criteria.

a high level of detail and clarity that can be deemed satisfactory in terms of contrast, sharpness, and noise level. Also, the generated images turn out to have a somewhat greater diagnostic utility, with an average qualitative rating of 7.43 out of 10. The images were found to be highly beneficial for clinical diagnostics and pathology identification, despite being artificial. Furthermore, the realism or authenticity of the simulated 3T MR images receive an average qualitative rating of 7.10 out of 10, indicating a strong resemblance to actual MRI scans in terms of anatomical precision and texture.

2) AVERAGE QUALITATIVE RATINGS FOR FAKE 7T MR IMAGES

The fake or generated 7T MRI scans receive a consistent assessment across all three categories, averaging 7.47 out of 10. The consistent rating indicates that the generated images perform at a high level in terms of quality, diagnostic utility, and realistic appearance or realism, slightly surpassing the generated 3T MR images according to the radiologists.

These findings highlight the efficacy of the CycleGAN model in producing synthetic MR images that closely resemble authentic MR images in both 3T and 7T. The qualitative ratings demonstrate a notable advancement in the authenticity and diagnostic effectiveness of the produced images, showcasing the potential of CycleGAN models in improving medical imaging technologies, especially medical image synthesis-based technologies.

I. LIMITATION AND FUTURE DIRECTIONS

This study was limited to T1-weighted MRI only. We wish to extend the present study to also work on T2-weighted MRI at 3T and 7T using CycleGAN. Future investigations should incorporate lesion detection into image translation for these types of image synthesis-based problems. Also, in future, we intend to implement novel loss functions, such as, dual contrast loss function [39], to further enhance the accuracy of the CycleGAN-generated images. Incorporating structural similarity index and cross-entropy into the dual contrast CycleGAN model could be advantageous as it takes into account both the brightness and structure of samples during picture synthesis [39]. These improvements have the

potential to greatly boost the quality and precision of the generated images.

In this work, we conducted experiments using just axial T1-weighted MRI scans at 3T and 7T. Our objective is to assist in the development and evaluation of techniques for translating MR images from 3T to 7T. Nevertheless, the CycleGAN models that were suggested were not trained to convert MR images into other planes, such as coronal and sagittal. Subsequent research could concentrate on extending the model to incorporate these planes, so offering a more all-encompassing method for translating MR images. In addition, we did not include any T2-weighted MRI scans. Subsequent research endeavors would strive to not only convert pictures between 3T and 7T, but also between T1 and T2-weighted images. This augmentation would enable the model to effectively process a broader range of MR imaging modalities, hence increasing its usefulness in clinical settings.

By acknowledging and overcoming these limits and investigating these potential areas of development, our aim is to make substantial progress in the skills and uses of CycleGAN-based MR image translation. Ultimately, this will contribute to enhancing the accuracy of diagnoses and effectiveness of treatments in medical imaging.

IV. CONCLUSION

Deep image synthesis is still in its infancy despite the fact that there have already been a number of studies on the subject, as it has many exciting new applications to explore over the next five to ten years [38]. Deep image synthesis techniques may also make it possible to develop innovative imaging modalities based on previously untapped physical processes [38].

This work aimed to assess the feasibility of using the CycleGAN model to convert MRI between two different field strengths. The study shows that the model has potential to generate realistic images for both domains according to several quantitative and qualitative evaluation criteria. Also, the performances of various architectures of CycleGAN have been investigated in detail on a novel dataset published recently. We have further shown that skull stripping post processing technique greatly boosted the performance of CycleGAN model to generate the target images.

ACKNOWLEDGMENT

The authors acknowledge the support from the Information and Communication Technology Division (ICTD), Ministry of Posts, Telecommunication and Information Technology, Government of the People's Republic of Bangladesh. This work was partially supported by the ICTP through the Affiliated Centers Program.

CONFLICT OF INTEREST

None of the authors have a conflict of interest to disclose.

REFERENCES

- [1] D. Nie, R. Trullo, J. Lian, L. Wang, C. Petitjean, S. Ruan, Q. Wang, and D. Shen, "Medical image synthesis with deep convolutional adversarial networks," *IEEE Trans. Biomed. Eng.*, vol. 65, no. 12, pp. 2720–2730, Dec. 2018.
- [2] G. Zeng and G. Zheng, "Hybrid generative adversarial networks for deep MR to CT synthesis using unpaired data," in *Proc. 22nd Int. Conf. Med. Image Comput. Comput. Assist. Intervent. (MICCAI)*, Shenzhen, China, Cham, Switzerland: Springer, Oct. 2019, pp. 759–767.
- [3] X. Chen, L. Qu, Y. Xie, S. Ahmad, and P.-T. Yap, "A paired dataset of T1- and T2-weighted MRI at 3 Tesla and 7 Tesla," *Sci. Data*, vol. 10, no. 1, p. 489, Jul. 2023.
- [4] P. E. Kinahan, D. W. Townsend, T. Beyer, and D. Sashin, "Attenuation correction for a combined 3D PET/CT scanner," *Med. Phys.*, vol. 25, no. 10, pp. 2046–2053, Oct. 1998.
- [5] K. Kyamakya, A. Bouchachia, J. C. Chedjou, and A. A. Hefnawy, "Super resolution challenges and rewards," in *Intelligence for Nonlinear Dynamics and Synchronisation*, 2010, pp. 163–206.
- [6] A. U. Zanzaney, R. Hegde, L. Jain, V. Rao, and C. K. Sharma, "Super resolution in medical imaging," in *Proc. Int. Conf. Netw., Multimedia Inf. Technol. (NMITCON)*, Oct. 2023, pp. 1–5.
- [7] H. Greenspan, "Super-resolution in medical imaging," *Comput. J.*, vol. 52, no. 1, pp. 43–63, Jan. 2009.
- [8] S. Farsiu, D. Robinson, M. Elad, and P. Milanfar, "Advances and challenges in super-resolution," *Int. J. Imag. Syst. Technol.*, vol. 14, no. 2, pp. 47–57, 2004.
- [9] C. Czobit and R. Samavi, "CycleGAN models for MRI image translation," 2023, *arXiv:2401.00023*.
- [10] R. Beisteiner, S. Robinson, M. Wurnig, M. Hilbert, K. Merksa, J. Rath, I. Höllinger, N. Klinger, C. Marosi, S. Trattinig, and A. Geißler, "Clinical fMRI: Evidence for a 7T benefit over 3T," *NeuroImage*, vol. 57, no. 3, pp. 1015–1021, Aug. 2011.
- [11] K. Bahrami, F. Shi, I. Rekić, and D. Shen, "Convolutional neural network for reconstruction of 7T-like images from 3T MRI using appearance and anatomical features," in *Proc. 1st Int. Workshop, 2nd Int. Workshop (DLMIA), Deep Learn. Data Labeling Medical Appl. (LABELS)*, Athens, Greece, Cham, Switzerland: Springer, Oct. 2016, pp. 39–47.
- [12] K. Bahrami, F. Shi, X. Zong, H. W. Shin, H. An, and D. Shen, "Hierarchical reconstruction of 7T-like images from 3T MRI using multi-level CCA and group sparsity," in *Proc. 18th Int. Conf. Med. Image Comput. Comput. Assist. Intervent. (MICCAI)*, Munich, Germany, Cham, Switzerland: Springer, Oct. 2015, pp. 659–666.
- [13] G. A. Kerchner, C. P. Hess, K. E. Hammond-Rosenbluth, D. Xu, G. D. Rabinovici, D. A. C. Kelley, D. B. Vigneron, S. J. Nelson, and B. L. Miller, "Hippocampal CA1 apical neuropil atrophy in mild Alzheimer disease visualized with 7-T MRI," *Neurology*, vol. 75, no. 15, pp. 1381–1387, Oct. 2010.
- [14] A. Radbruch, O. Eidel, B. Wiestler, D. Paech, S. Burth, P. Kickingereder, M. Nowosielski, P. Bäumer, W. Wick, H.-P. Schlemmer, M. Bendzus, M. Ladd, A. M. Nagel, and S. Heiland, "Quantification of tumor vessels in glioblastoma patients using time-of-flight angiography at 7 Tesla: A feasibility study," *PLoS ONE*, vol. 9, no. 11, Nov. 2014, Art. no. e110727.
- [15] Z.-H. Cho, H.-K. Min, S.-H. Oh, J.-Y. Han, C.-W. Park, J.-G. Chi, Y.-B. Kim, S. H. Paek, A. M. Lozano, and K. H. Lee, "Direct visualization of deep brain stimulation targets in Parkinson disease with the use of 7-Tesla magnetic resonance imaging," *J. Neurosurgery*, vol. 113, no. 3, pp. 639–647, Sep. 2010.
- [16] M. Cosottini and L. Roccatagliata, "Neuroimaging at 7 T: Are we ready for clinical transition?" *Eur. Radiol. Exp.*, vol. 5, no. 1, p. 37, 2021.
- [17] Y. Zhang, P.-T. Yap, L. Qu, J.-Z. Cheng, and D. Shen, "Dual-domain convolutional neural networks for improving structural information in 3 T MRI," *Magn. Reson. Imag.*, vol. 64, pp. 90–100, Dec. 2019.
- [18] A. E. Campbell-Washburn et al., "Opportunities in interventional and diagnostic imaging by using high-performance low-field-strength MRI," *Radiology*, vol. 293, no. 2, pp. 384–393, Nov. 2019.
- [19] C. N. Wiens, C. T. Harris, A. T. Curtis, P. J. Beatty, and J. A. Stainsby, "Feasibility of diffusion tensor imaging at 0.5 T," presented at the Int. Soc. Magn. Reson. Med. (ISMRM) Conf., 2020. [Online]. Available: <https://www.synaptivemedical.com/wp-content/uploads/2020/08/Feasibility-of-Diffusion-Tensor-Imaging-at-0.5T.pdf>
- [20] M. Hayat, S. Aramvith, and T. Achakulvisut, "Combined channel and spatial attention-based stereo endoscopic image super-resolution," in *Proc. IEEE Region 10 Conf. (TENCON)*, Oct. 2023, pp. 920–925.
- [21] M. Hayat, S. Aramvith, and T. Achakulvisut, "SEGSNet for stereo-endoscopic image super-resolution and surgical instrument segmentation," 2024, *arXiv:2404.13330*.
- [22] M. Hayat and S. Aramvith, "E-SEVSR—Edge guided stereo endoscopic video super-resolution," *IEEE Access*, vol. 12, pp. 30893–30906, 2024.
- [23] X. Yi, E. Walia, and P. Babyn, "Generative adversarial network in medical imaging: A review," *Med. Image Anal.*, vol. 58, Dec. 2019, Art. no. 101552.
- [24] S. Kazemina, C. Baur, A. Kuijper, B. van Ginneken, N. Navab, S. Albarqouni, and A. Mukhopadhyay, "GANs for medical image analysis," *Artif. Intell. Med.*, vol. 109, Sep. 2020, Art. no. 101938.
- [25] I. J. Goodfellow, J. Pouget-Abadie, M. Mirza, B. Xu, D. Warde-Farley, S. Ozair, A. Courville, and Y. Bengio, "Generative adversarial networks," *Commun. ACM*, vol. 63, no. 11, pp. 139–144, 2020.
- [26] J.-Y. Zhu, T. Park, P. Isola, and A. A. Efros, "Unpaired image-to-image translation using cycle-consistent adversarial networks," in *Proc. IEEE Int. Conf. Comput. Vis. (ICCV)*, Oct. 2017, pp. 2242–2251.
- [27] L. Qu, Y. Zhang, S. Wang, P.-T. Yap, and D. Shen, "Synthesized 7T MRI from 3T MRI via deep learning in spatial and wavelet domains," *Med. Image Anal.*, vol. 62, May 2020, Art. no. 101663.
- [28] C.-B. Jin, H. Kim, M. Liu, W. Jung, S. Joo, E. Park, Y. Ahn, I. Han, J. Lee, and X. Cui, "Deep CT to MR synthesis using paired and unpaired data," *Sensors*, vol. 19, no. 10, p. 2361, May 2019.
- [29] H. Do, P. Bourdon, D. Helbert, M. Naudin, and R. Guillevin, "7T MRI super-resolution with generative adversarial network," *Electron. Imag.*, vol. 33, no. 18, pp. 106-1–106-7, Jan. 2021.
- [30] O. Esteban, D. Birman, M. Schaer, O. O. Koyejo, R. A. Poldrack, and K. J. Gorgolewski, "MRIQC: Advancing the automatic prediction of image quality in MRI from unseen sites," *PLoS ONE*, vol. 12, no. 9, Sep. 2017, Art. no. e0184661.
- [31] E. Branikas, P. Murray, and G. West, "A novel data augmentation method for improved visual crack detection using generative adversarial networks," *IEEE Access*, vol. 11, pp. 22051–22059, 2023.
- [32] D. Brunet, E. R. Vrscaj, and Z. Wang, "On the mathematical properties of the structural similarity index," *IEEE Trans. Image Process.*, vol. 21, no. 4, pp. 1488–1499, Apr. 2012.
- [33] C. Plapous, C. Marro, and P. Scalart, "Improved signal-to-noise ratio estimation for speech enhancement," *IEEE Trans. Audio, Speech Lang. Process.*, vol. 14, no. 6, pp. 2098–2108, Nov. 2006.
- [34] P. Händel, "Understanding normalized mean squared error in power amplifier linearization," *IEEE Microw. Wireless Compon. Lett.*, vol. 28, no. 11, pp. 1047–1049, Nov. 2018.
- [35] L. Mendo, "Estimation of a probability with guaranteed normalized mean absolute error," *IEEE Commun. Lett.*, vol. 13, no. 11, pp. 817–819, Nov. 2009.
- [36] X.-H. Zhou, G.-B. Bian, X.-L. Xie, Z.-G. Hou, R.-Q. Li, and Y.-J. Zhou, "Qualitative and quantitative assessment of technical skills in percutaneous coronary intervention: In vivo porcine studies," *IEEE Trans. Biomed. Eng.*, vol. 67, no. 2, pp. 353–364, Feb. 2020.
- [37] K. Nishimaki, K. Ikuta, S. Fujiyama, K. Oishi, and H. Iyatomi, "PCSS: Skull stripping with posture correction from 3D brain MRI for diverse imaging environment," *IEEE Access*, vol. 11, pp. 116903–116918, 2023.
- [38] G. Wang, J. C. Ye, and B. De Man, "Deep learning for tomographic image reconstruction," *Nature Mach. Intell.*, vol. 2, no. 12, pp. 737–748, Dec. 2020.
- [39] J. Wang, Q. M. J. Wu, and F. Pourpanah, "DC-cycleGAN: Bidirectional CT-to-MR synthesis from unpaired data," *Computerized Med. Imag. Graph.*, vol. 108, Sep. 2023, Art. no. 102249.



ZAKARIA SHAMS SIAM received the Bachelor of Science degree in computer science and engineering (major) and mathematics (minor) from the Department of Electrical and Computer Engineering, North South University, Dhaka, Bangladesh. He is currently pursuing the M.Sc. (Full Research) degree with the Department of Electrical, Electronic and Systems Engineering, Faculty of Engineering and Built Environment, Universiti Kebangsaan Malaysia (UKM), Bangi, Malaysia. He has published several international journal articles, book chapters, and conference proceedings. His current research interests include artificial intelligence, machine learning, and computer vision.



RUBYAT TASNUVA HASAN received the B.Sc. degree in computer science and engineering from the Department of Electrical and Computer Engineering, North South University, Bangladesh. She is currently a Researcher. She has published several international journal articles, book chapters, and conference proceedings. Her current research interests include artificial intelligence and machine learning.



ADAM MUSHTAK received the M.D. degree from Weill Cornell Medicine, Qatar, in 2019. He is a Medical Professional dedicated to innovation and progress. He is the Chief Resident with the Diagnostic and Interventional Radiology Residency Program, Hamad Medical Corporation, Qatar. His research interests include the integration of machine learning and artificial intelligence in clinical imaging, reflecting his commitment to advancing healthcare. Eager to contribute to the field, he looks forward to pursuing a Fellowship in Nuclear and Molecular Medicine to deepen his expertise.



MOAJJEM HOSSAIN CHOWDHURY received the B.Sc. degree in electrical and electronics engineering from North South University, Bangladesh. He is currently pursuing the M.Sc. degree with Universiti Kebangsaan Malaysia (UKM). He is a Research Assistant with Qatar University (QU). His current research interests include biomedical signal processing, machine learning, and data science. He placed in the top 30 in Bangladesh Physics Olympiad 2014.



ISRAA AL-HASHIMI received the M.D. degree from Qatar University College of Medicine, in 2021. Currently, she is a Radiology Resident with Hamad Medical Corporation. She is deeply committed to advancing the field of radiology. Her research interests extend to diagnostic and interventional radiology, artificial intelligence in medicine, medical education, and community medicine. Furthermore, she is passionate about radiology research, with a focus on neuroradiology and neuroscience, aiming to contribute to both medical knowledge and patient care in these specialized areas.



MD. SHAHEENUR ISLAM SUMON is currently pursuing the Graduate degree in biomedical engineering. He is also a Research Assistant with the Machine Learning Group, Qatar University.



SOHAIB BASSAM ZOGHOUL received the M.B.B.S. degree from Jordan University of Science and Technology. Currently, he is a Doctor engaged in a residency program, specializing in interventional and diagnostic radiology with Hamad Medical Corporation, Doha, Qatar. He has a special interest in radiology related artificial intelligence and machine learning research field.



MAMUN BIN IBNE REAZ (Senior Member, IEEE) received the D.Eng. degree from Ibaraki University, Mito, Japan, in 2007. He is currently a Professor with Independent University in Bangladesh, Dhaka, Bangladesh. He is the author or co-author of more than 400 research articles in design automation, integrated circuit (IC) design for biomedical applications, and smart home.



MUHAMMAD E. H. CHOWDHURY (Senior Member, IEEE) received the Ph.D. degree from the University of Nottingham, U.K., in 2014. He was a Postdoctoral Research Fellow with the Sir Peter Mansfield Imaging Centre, University of Nottingham. He is currently an Assistant Professor and a Program Coordinator of the Department of Electrical Engineering, Qatar University. He has filed several patents and published more than 200 peer-reviewed journal articles, more than 30 conference papers, and several book chapters. He is currently running NPRP, UREP, and HSREP grants from Qatar National Research Fund (QNRF) and internal grants (IRCC and HIG) from Qatar University along with academic projects from HBKU and HMC. His current research interests include biomedical instrumentation, signal processing, wearable sensors, medical image analysis, machine learning and computer vision, embedded system design, and simultaneous EEG/fMRI. He is a member of British Radiology, ISMRM, and HBM. He has recently won the COVID-19 Dataset Award, the AHS Award from HMC, and the National AI Competition Awards for his contribution to the fight against COVID-19. His team was the gold-medalist in the 13th International Invention Fair in the Middle East (IIFME). He has been listed among the Top 2% of scientists in the World List, published by Stanford University. He is serving as a Guest Editor for *Polymers*, an Associate Editor for *IEEE Access*, and a Topic Editor and a Review Editor for *Frontiers in Neuroscience*.



SAWAL HAMID BIN MD ALI (Senior Member, IEEE) received the M.Sc. and Ph.D. degrees from the University of Southampton, Southampton, U.K., in 2004 and 2010, respectively. He is currently a Professor of embedded systems with the Department of Electrical, Electronic and Systems Engineering, Faculty of Engineering and Built Environment, Universiti Kebangsaan Malaysia (UKM), Bangi, Malaysia. His current research interests include wearable systems, system-on-chip design, and pervasive computing.

...